Characterisation of oxide scale adherence after the high temperature oxidation of nickel-based superalloys

Elena Fedorova[a,b]*, Daniel Monceau[b], Djar Oquab[b] and Alexandre Popov[a]

[a]*Polytechnic Institute of Siberian Federal University, 660074 Krasnoyarsk, Russia*

[b]*Institut Carnot CIRIMAT, ENSIACET, BP-44362, Allée Emile Monso, 31030 Toulouse cedex-4, France*

**E-mail: fedorova.elena.85@gmail.com*

ABSTRACT

The scratch test technique was used to characterise the adherence of multi-layered oxide scales formed during the high temperature isothermal oxidation (1100°C) of a single crystal Ni-based superalloy AM1 with varying sulfur concentrations (0.22–3.2 ppmw). Results were discussed in relation to cyclic oxidation behaviour and microstructural evolution of oxidised samples. The most commonly used elastic energy-based models were applied to calculate the work of adhesion. The obtained values of the work of adhesion were then analysed with regard to the mode-dependence of the fracture behaviour and the possible sources of errors in the scratch test results interpretation. This analysis allowed us to understand the limits of validity of these models and of the experimental value of the work of adhesion.

Keywords: nickel-based superalloys, oxidation, interface, adhesion energy

INTRODUCTION

Applications of the scratch test technique for adhesion analysis have been developed and reported in many studies [1–13], in particular, for thermally grown oxide on the surface of heat-resistant alloys [9].

In a previous work [14], the ability of the scratch test to quantify the adherence of oxide scale formed on Ni-base superalloys after short term isothermal oxidation was evaluated. However, the mechanical behaviour of thin film/substrate systems under sliding indenter loading is complex. Difficulties include a complicated stress–strain field, different failure modes occurring at the same time, and numerous intrinsic and extrinsic parameters [5–10]. Therefore, the interpretation of scratch test results to determine the values of adhesion work, which is a parameter for the quantitative evaluation of the adhesion strength between oxide scale and a substrate, can be misleading.

In order to correctly assess the work of adhesion using the scratch technique and to understand the limits of validity of the results, the most commonly used models were chosen as the basis for the adhesion analysis of Ni-based sureralloys with different sulfur concentrations.

MATERIALS AND METHODS

Single crystal Ni-base first-generation superalloys AM1, with different sulfur concentrations, were provided by Snecma-Safran Group. The sulfur content ranged from 0.22 up to 3.2 ppmw, as measured by glow-discharge mass spectroscopy (GDMS). The chemical composition of the superalloy is presented in Table 1. Disk-shape samples of 11–13 mm diameter and 1 mm thick were machined along the [001] direction from rods. Prior to oxidation, all sides of the specimens were ground and polished down to a 1-μm surface finish, then samples were cleaned in an ultrasonic bath with acetone followed by high-purity alcohol. They were weighed to within 10 μg with a Sartorius ME balance before and after high-temperature exposures.

The isothermal thermogravimetric tests were performed in a SETARAM® TAG 24S thermobalance with sensitivity greater than 1 μg which is suitable for the accurate measure-

Table 1 Chemical composition of the single-crystal Ni-based superalloy AM1 (wt%)

Alloys	S (ppmw)	Cr	Co	Mo	W	Ta	Al	Ti	Re	Ru	Hf	Ni
AM1	0.22 0.41 3.20	7.5	6.5	2	5.5	8	5.3	1.2	–	–	–	Base

doi: 10.3184/096034012X13343145866993

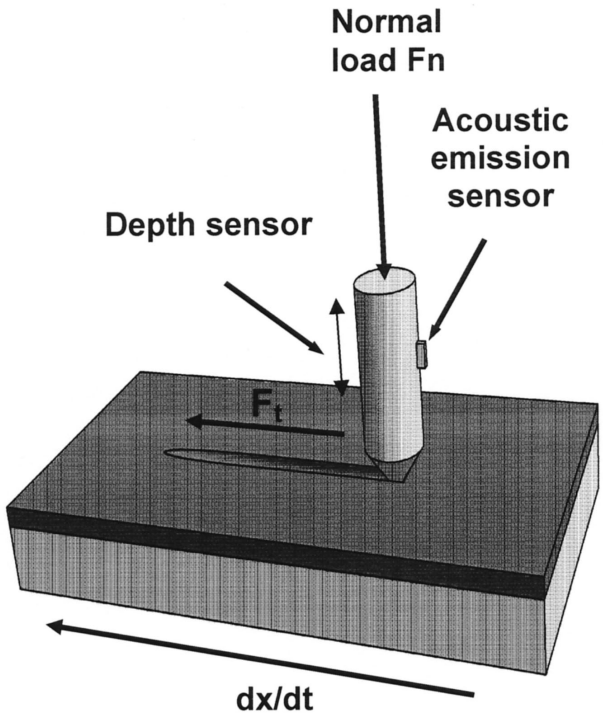

Figure 1 Schematic representation of the scratch test.

ment of small mass changes. The samples were oxidised at 1100°C achieved with a heating rate of 60°C min^{-1} in synthetic air whose flow rate was maintained at 0.4 L h^{-1}. The specimens with three different sulfur levels were oxidised for 9, 17 and 18 h to form oxide scales of similar thickness. The continuous recording of the mass gain within the thermobalance allowed the experiments to be stopped when the desired oxide scale thickness was reached. It also allowed the detection of spalling during cooling. In the present case, no spalling event was detected. The total oxide scale thickness (t) was determined from the difference of the mass before oxidation and at the end of the process inside the thermobalance, *i.e.* at room temperature. The value of t was then verified from the direct observation using scanning electron microscopy (SEM) on a LEO 435VP system in conventional mode. The microstructures of the oxide scales formed on AM1 were characterised using back-scattered and secondary electron modes. The oxide phases were identified by X-ray diffraction (XRD) using a Seifert 3000TT diffractometer. Chemical analysis by means of a PGT (imix-PC) system for the EDS was performed as a complementary study.

Cyclic oxidation tests were conducted in a previous study on specimens coming from the same alloy batch [15]. A thermal cycle consisted of a fast heating period at 90°C min^{-1} up to 1100°C (transfer of the samples to the hot zone in 10 s), a 60 min exposure at 1100°C (including heating) in laboratory air, followed by a 15 min fast cooling to room temperature in a strong flow of purified air.

To evaluate the mechanical adherence of the oxide scale formed on AM1 alloys, the scratch test was carried out using a commercial SCM Revetest scratch tester. A Rockwell diamond indenter with a 200 μm radius hemispherical tip was used. The normal load F_n was continuously increased from 1 N up to 100 N. The loading rate was 50 N min^{-1}. A 3 mm long scratch was made during each test. The instrument is equipped with an integrated optical microscope, an acoustic emission monitoring system to detect crack formation and a device to measure the horizontal frictional force F_t in the scratching direction from which the friction coefficient values μ can be obtained ($F_t = \mu F_n$). The critical load criterion used was the lowest load at which failure occurred along the scratch track, as determined by optical microscope examination. The first acoustic emission peak observed and the variation of the frictional force provide complementary information for critical load measurements. Five scratches were performed on each sample under the test conditions determined previously. Average values of critical normal load, corresponding frictional force, coefficient of friction, and track width are reported. A schematic representation of test is shown in Figure 1. As already established [6,7,10], the critical load is factored by intrinsic parameters, including loading rate and scratch velocity. In the present study, the operating parameters of the scratch test were determined previously and were fixed.

RESULTS AND DISCUSSION

Isothermal oxidation and characterisation of microstructure

Results for isothermal oxidation of AM1 at 1100°C show faster oxidation kinetics over the transient regime for all the samples [14]. After approximately 6 h, the oxidation kinetics follows a parabolic law. Moreover, the oxidation kinetics of AM1 specimens was not monotonous functions of the sulfur level. The highest oxidation kinetics was found for the sample with the intermediate sulfur level. This result can be explained in terms of materials processing differences resulting in different impurity levels for this series of rods, but no precise data are available [14].

Back-scattered and secondary electron images of the oxide scales formed on the surface of AM1 alloy at 1100°C are presented in Figure 2. The multi-layered oxide consists of an inner alumina layer in contact with the metal and an outer $NiAl_2O_4$ spinel layer separated by discontinuous (Ta, Ti)-rich oxide (bright spots on BSE images Figure 2b). TiO_2 was also identified by XRD so the (Ta–Ti)-rich oxide is certainly a rutile phase.

Assessment of the work of adhesion of oxide scales using the scratch technique

A detailed analysis of energy-based models to assess the work of adhesion using the scratch test technique has been reported elsewhere [14]. The differences between two models used in the present work are based on the method employed for the evaluation of the local stress.

Indeed, the scratch test implies deformation of the material in elastic and plastic forms until the coating and substrate are separated. Burnett and Rickerby developed the analysis based on the elastic–plastic indentation theory [7,8] and identified three components for the total stress responsible for coating detachment during the scratch test. First, a static

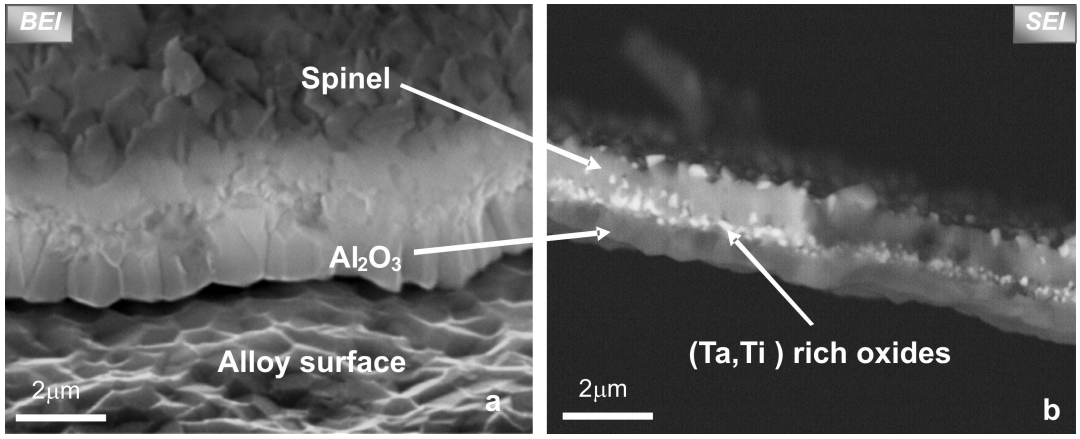

Figure 2 SEM micrographs of the oxide scales formed on AM1 after isothermal oxidation at 1100°C in synthetic air.

elastic–plastic indentation stress, second, a tangential frictional stress due to the interaction between the sliding indenter and the specimen surface and third, the residual internal stresses in the film. This analysis was extended by Bull *et al*. [16] and later refined by Bull and Rickerby [17]. Each one of the three contributions described before was expressed in terms of its effect on the measured total frictional force F_t. Indentation stress has been considered as the component of stress responsible for film delamination. Accordingly, the local compressive stresses in the plane of the interface or the tensile stresses normal to the interface, due to Poisson's effect, cause the oxide/scale detachment. The final equation which relates the minimum critical load with the practical work of adhesion, W, is:

$$W = \mu_c^2 F_{nc}^2 \cdot \frac{v_f^2 t}{2A^2 E_f} \tag{1}$$

Where v_f and E_f are the Poisson ratio and Young's modulus of the film; $\mu_c = F_t/F_{nc}$ is the friction coefficient corresponding to the critical load; A is the cross-sectional area of the track, which can be calculated using the indenter radius R and the track width d_c measured at critical load F_{nc}:

$$A = R^2 \sin^{-1}\left(\frac{d_c}{2R}\right) - \frac{d_c}{2}\left[R^2 - \left(\frac{d_c}{2}\right)^2\right]^{1/2}$$

This model has been modified by Attar and Johanneson [11] using an equation which, in contrast to Eqn (1), shows an indirect proportionality between the work of adhesion and the coating thickness:

$$W = \left(\frac{v_f \mu_c F_{nc}}{d_c}\right)^2 \cdot \frac{1}{2E_f t} \tag{2}$$

A combination of shear and tensile stresses in the coating/substrate interface ahead of the indenter and the possibility of plastic deformation occurring in the coating were assumed. In this model, the frictional force acts on the cross-section of the coating $A = td_c$ [11].

Before applying these models to the oxidised superalloys, the failure modes which have occurred during the scratch tests were analysed. For the studied oxide scale/substrate test were observed during the scratch track examination. First, the interfacial spallation at the border of the scratch track and second, the conformal type buckling cracks. In many cases, it is difficult to identify the predominant failure mode.

For the oxide scales with a constant thickness and a surface finish of 1 μm, different critical normal and tangential forces were measured depending on the sulfur level. There was a clear tendency for the critical load to decrease with increasing sulfur content. AM1 containing 0.22 ppmw S [Figure 3(a) and (c)] was considerably more resistant to detachment in comparison with 3.2 ppmw S sample. Optical observations of detachment development show large areas of spallation at early load for the oxide scale grown on alloy with the highest sulfur levels of 3.2 ppmw S [Figure 3(b) and (d)]. At the end of the test, the oxide scale was completely removed from the substrate.

The work of adhesion was estimated using the models described in Eqns (1) and (2) (models 1 and 2 correspondingly), and assuming the following elastic properties for the oxide scale: Young's modulus of bulk alumina $E_f = 380$ GPa, and Poisson ratio $v_f = 0.24$ [18].

The obtained results are presented in Table 2. Both models show a tendency towards a decreasing work of adhesion with increasing sulfur content. These qualitative and quantitative results are in good accordance with the cyclic oxidation kinetics reported in Figure 4 and numerous data reported in the literature [19–21]. The role of sulfur is likely to be associated with a reduction in fracture toughness of the oxide/metal interfaces through formation of voids or reduction of the bonding energy [21]. According to Table 2, the values of the work of adhesion calculated with the model of Bull and Rickerby [Eqn (1)] are very small in comparison with those given in Attar and Johanneson's model [Eqn (2)]. For example, for specimen 1, the value of W given by Eqn (1) was 2.2 J m^{-2} and by Eqn 2 was 21.7 J m^{-2}. This fact can be explained by the differences in the mode of loading assumed in Eqn (1) and (2) changing from mode I to II accordingly. Model 1 assumes that the oxide/scale detachment is caused by the tensile stresses normal to the interface, whereas model 2 assumes a combination of shear and tensile stresses in the coating/substrate interface.

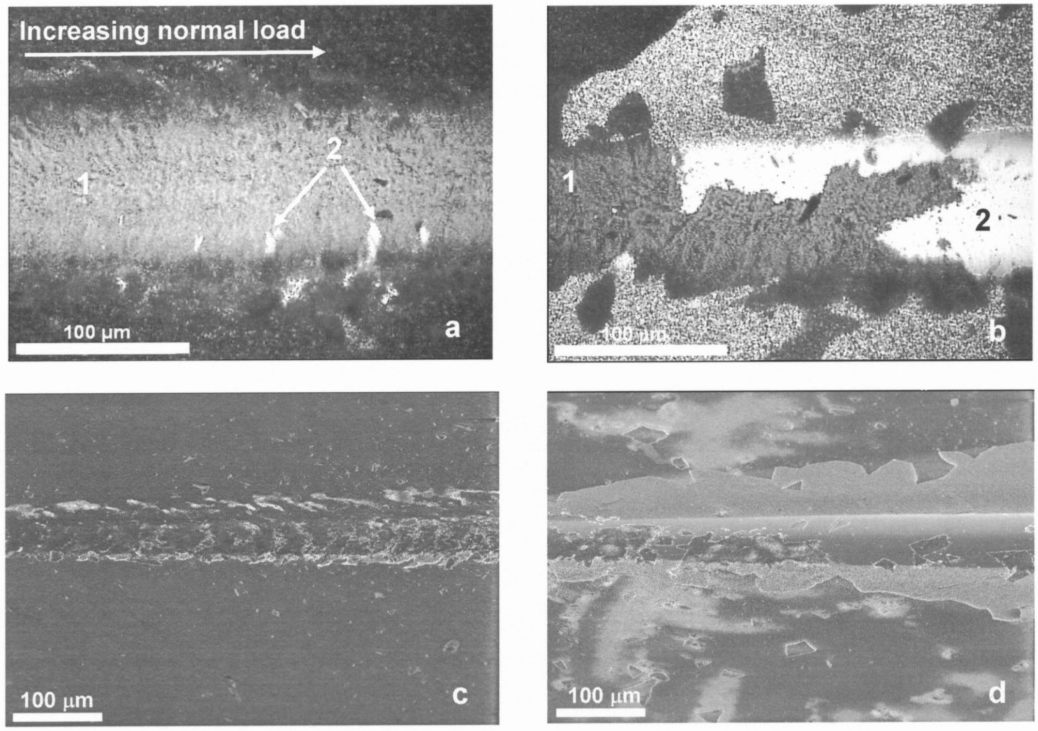

Figure 3 Optical (**a**, **b**) and SEM (**c**, **d**) micrographs showing the oxide scale spalling induced by the scratch test for AM1 samples with two sulfur contents 0.22 ppmw (**a**, **c**) and 3.2 ppmw (**b**, **d**): 1 – oxide scales; 2 – alloy surface.

It is obvious from Eqns (1) and (2) that the W values are strongly affected by the magnitude of Young's modulus and the Poisson ratio. Young's modulus values for TGO alumina vary between 350 and 400 GPa, this can result in errors in W values of less than 10% and 8% calculated using Eqns (1) and (2) respectively. The variations of Poisson ratio v_f values can lie between 0.2 and 0.28 according to the data reported for thermally grown α-Al_2O_3 [22]. Moreover, the film is represented by multilayered oxides. This uncertainty in the value of the Poisson ratio leads to errors of about 30 – 50%. On the other hand, an error of about 10% may also arise from incorrect track width d measurement ($\pm$ 5 μm). Therefore, the expected total error is 50 – 70%, which is still not as large as the effect of the internal residual stress in the oxide scale.

For the values presented in Table 2, scale residual stresses σ_R, were not considered. In our case, the tilted surfaces of oxidised superalloys after spalling were analysed and no wrinkling nor cavity formation was observed. The most obvious observation was the multi-layered nature of the oxide scale. Nevertheless, if it is assumed that the oxide scale has the same elastic and dilatation properties as α-Al_2O_3, the value of the TGO residual stresses can be estimated from the thermal expansion mismatch between the thin oxide layer and the thick substrate [23]. The thermal stresses, in first approximation, were then estimated using Eqn (3):

$$\sigma_R = -\frac{E_f \Delta T \Delta\alpha}{(1 - v_f)} \tag{3}$$

where ΔT is temperature change; $\Delta\alpha = \alpha_s - \alpha_f$ is the difference in thermal expansion coefficients of the substrate (~13 – 16 C^{-1} ppm) and the oxide scale (~8 – 9 C^{-1} ppm). Temperature dependence of E_f and α was ignored. Accordingly, calculated average compressive stress values of σ_R are between -2.7 and -3.8 GPa. Experimentally measured values of residual stresses in the alpha alumina scale using XRD, optical fluorescence spectroscopy (OFS)

Table 2 Average values of critical load measured during the scratch test and calculated values of the work of adhesion for AM1 samples polished down to 1 μm finish

AM1 sample No.	Sulfur content (ppmw)	Oxide scale thickness t[a] (μm)	Critical load F_{nc}, (N)	Work of adhesion W, (J m^{-2})	
				Model 1	Model 2
1	0.22	1.1	19.5 ± 1.1	2.2	21.7
2	0.41	1.3	14.6 ± 1.2	2.0	11.4
3	3.2	1.3	10.0 ± 0.5	1.8	6.5

Five scratches were performed for each sample.
[a]Calculated from TGA data.

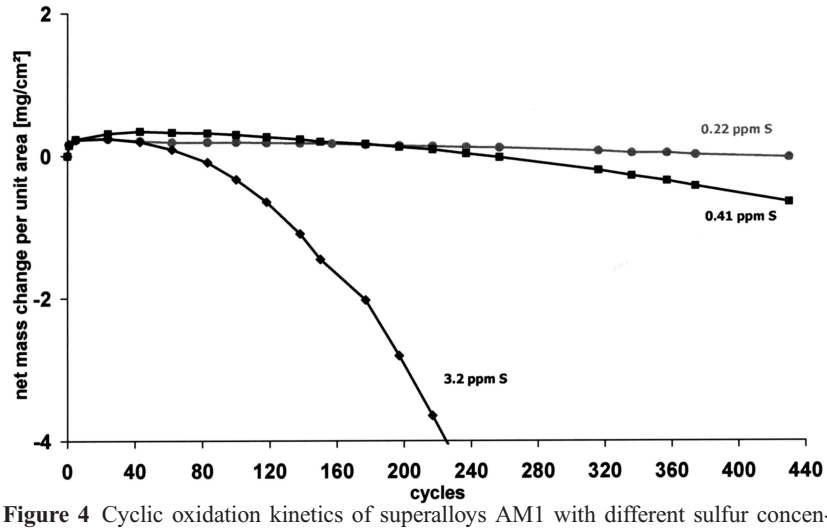

Figure 4 Cyclic oxidation kinetics of superalloys AM1 with different sulfur concentrations (1 h cycles at 1100°C) [15].

and photo-simulated luminescence spectroscopy (PSLS) vary between -3 and -6 GPa depending on substrate and oxidation conditions [9,24,25]. Taking a representative value of $\sigma_R = -4$ GPa (assuming that the internal stress remains constant) and addition of the measured compressive failure stress, allows us to calculate the work of adhesion values presented in Table 3. These values show the same trend for the specimens with the same oxide thickness but different S levels, but are appreciably higher than the previous calculation, which neglected internal stresses. As a representative example, the values of W for specimen 1 without σ_R are 2.2 J m^{-2} [Eqn (1)] and 21.7 J m^{-2} [Eqn (2)]. With σ_R, the values increase to 39.1 and 90.3 J m^{-2} respectively. This clearly shows that the evaluation of scale residual stress is crucial to calculating the work of adhesion.

It is important to point out that both models use only the physical properties of the oxide film. The properties of the substrate are not incorporated into these models. The mechanism of delamination during the scratch test is much more complex and should take into consideration the effect of substrate plastic deformation and stress state in the local contact zone between the indenter and the scratched surface.

The values of work of adhesion obtained in the present study using the scratch test were compared to results obtained using the scratch test and other techniques for other thermally grown oxide scales on an alloy substrate. The order of magnitude of values obtained in the present study agrees with previous investigations [9,26–29]. We have related a relatively large distribution of values with different fracture behaviour modes and reported the fracture energy of alloy/alumina interfaces determined by a variety of methods to be between ~5 and 110 J m^{-2} increasing from mode I to II accordingly.

CONCLUSION

The two models used to assess the adhesion work show the same variation with sulfur content decreasing the adhesion of alumina scale on the AM1 superalloy, which is in accordance with cyclic oxidation behaviour. However, the models lead to different values for the adhesion work, which could be explained by the differences in the mode of loading assumed in two models. The evaluation of scale residual stress is crucial to the calculation of the work of adhesion.

Nevertheless, the scratch test, undertaken under careful conditions on isothermally oxidised samples, could be used to predict qualitatively the long-term cyclic oxidation behaviour of samples with varying chemical compositions.

The focus of the future work will be to develop a new model able to dissociate the effects of oxidation time and the affect of oxide scale thickness on the value of the energy of adhesion taking into consideration the residual stresses and the effect of substrate plastic deformation.

ACKNOWLEDGEMENTS

The authors gratefully acknowledge Diane Samelor (CIRIMAT laboratory) for her help with the scratch tests; Snecma-Safran Group (France) for providing samples of superalloys.

REFERENCES

[1] Volinsky, A.A., Moody, N.R. and Gerberich, W.W. (2002) Interfacial toughness measurements for thin films on substrates. *Acta Mater.*, **50**, 441–466.
[2] Benjamin, P. and Weaver, C. (1960) Measurement of adhesion of thin films. *Proc. R. Soc. A*, **254**, 163–176.

Table 3 Calculated values of the work of adhesion with or without considering the residual stresses

AM1, sample No.	Model 1			Model 2		
	Failure stress, (GPa)	Work of adhesion W (J m^{-2})		Failure stress, (GPa)	Work of adhesion W (J m^{-2})	
		Without σ_R	With σ_R		Without σ_R	With σ_R
1	1.2	2.2	39.1	3.9	21.7	90.3
2	1.1	2.0	44.5	2.6	11.4	74.5
3	1.8	1.8	42.8	1.9	6.5	59.5

[3] Perry, A.J. (1983) Scratch adhesion testing of hard coatings. *Thin Solid Films*, **107**, 167–180.

[4] Laugier, M.T. (1984) An energy approach to the adhesion of coating using the scratch test. *Thin Solid Films*, **117**, 243–249.

[5] Valli, J., Makela, U., Matthews, M. and Murawa, V. (1985) A review of adhesion test methods for thin hard coatings. *J. Vac. Sci. Technol*., **A36**, 2411–2414.

[6] Steinmann, P.A., Tardy, Y. and Hintermann, H.E. (1987) Adhesion testing by the scratch test method: the influence of intrinsic and extrinsic parameters on the critical load. *Thin Solid Films*, **154**, 403–416.

[7] Burnett, P.J. and Rickerby, D.S. (1987) The relationship between hardness and scratch adhesion. *Thin Solid Films*, **148**, 41–50.

[8] Burnett, P.J. and Rickerby, D.S. (1988) The scratch adhesion test: an elastic-plastic indentation analysis. *Thin Solid Films*, **157**, 233–254.

[9] Bull, S.J. (1997) Failure mode maps in the thin film scratch adhesion test. *Tribol. Int*., **30**, 491–498.

[10] Bull, S.J. and Berasetegui, E.J. (2006) An overview of the potential of quantitative coating adhesion measurement by scratch testing. *Tribol. Int*., **39**, 99–114.

[11] Attar, F. and Johannesson, T. (1996) Adhesion evaluation of thin ceramic coatings on tool steel using the scratch testing technique. *Surf. Coat. Technol*., **78**, 87–102.

[12] Xie, Y. and Hawthorne, H.M. (2001) Effect of contact geometry on the failure modes of thin coatings in the scratch adhesion test. *Surf. Coat. Technol*., **141**, 15–25.

[13] Holmberg, K., Laukkanen, A., Ronkainen, H., Wallini, K. and Varjus, S. (2003) A model for stresses, crack generation and fracture toughness calculation in scratched TiN-coated steel surfaces. *Wear*, **254**, 278–291.

[14] Fedorova, E., Monceau, D. and Oquab, D. (2010) Quantification of growth kinetics and adherence of oxide scales formed on Ni-based superalloys at high temperature. *Corros. Sci*., **52**, 3932–3942.

[15] Ast, J., Monceau, D. and Oquab, D. (2007) CIRIMAT Toulouse.

[16] Bull, S.J., Rickerby, D.S., Matthews, A., Leyland, A., Pace, A.R. and Valli, J. (1988) The use of scratch adhesion testing for the determination of interfacial adhesion. The importance of frictional drag. *Surf. Coat. Technol*., **36**, 503–517.

[17] Bull, S.J. and Rickerby, D.S. (1990) New developments in the modelling of the hardness and scratch adhesion of thin films. *Surf Coat. Technol*., **42**, 149–164.

[18] Morrell, R. (1987) *Handbook of properties of technical and engineering ceramics*, HMSO, London.

[19] Smeggil, J.G., Funkenbush, A.W. and Bornstein, N.S. (1986) A relationship between indigenous impurity elements and protective oxide scale adherence characteristics. *Metall. Trans*., **A17**, 923–932.

[20] Hou, P.Y. and Stringer, J. (1992) Oxide scale adhesion and impurity segregation at the scale/metal interface. *Oxid. Met*., **38**, 323–345.

[21] Nychka, J.A., Clarke, D.R. and Meier, G.H. (2008) Spallation and transient oxide growth on PWA 1484 superalloy. *Mater. Sci. Eng*., **A490**, 359–368.

[22] Evans, A.G., Hutchinson, J.W. and He, M.Y. (1999) Micromechanics model for the detachment of residually compressed brittle films and coatings. *Acta Mater*., **47**(5), 1513–1522.

[23] Tien, K. and Davidson, J.M. (1975) Oxide spallation mechanisms. Stress effects and the oxidation of metals. J. V. Cathcart. *AIME*, 200–219.

[24] Schumann, E., Sarioglu, C., Blachere, J.R., Pettit, F.S. and Meier, G.H. (2000) High-temperature stress measurements during the oxidation of NiAl. *Oxid. Met*., **53**, 259–272.

[25] Lipkin, D.M., Clarke, D.R., Hollatz, M., Bobeth, M. and Pompe, W. (1997) Stress development in alumina scales formed upon oxidation of (111) NiAl single crystals. *Corros. Sci*., **39**, 231–242.

[26] Mennicke, C., He, M.-Y., Clarke, D.R. and Smith, J.S. (2000) The role of secondary oxide inclusions ("pegs") on the spalling resistance of oxide films. *Acta Mater*., **48**, 2941–2949.

[27] Begley, M.R., Mumm, D.R., Evans, A.G. and Hutchinson, J.W. (2000) Analysis of a wedge impression test for measuring the interface toughness between films/coatings and ductile substrates. *Acta Mater*., **48**, 3211–3220.

[28] Théry, P.-Y., Poulain, M., Dupeux, M. and Braccini, M. (2007) Adhesion energy of a YPSZ EB-PVD layer in two thermal barrier coating systems. *Surf. Coat. Technol*., **202**, 648–652.

[29] Bamba, G., Wouters, Y., Galerie, A., Charlot, F. and Dellali, A. (2006) Thermal oxidation kinetics and oxide scale adhesion of Fe15Cr alloys as a function of their silicon content. *Acta Mater*., **54**, 3917–3922.